# Meta-stable Magnetic Exchange Spring States with Negative Coercivity in $DyFe_2/YFe_2$ Multilayers

D. Wang[a], A.R. Buckingham[a], G.J. Bowden[a], R.C.C. Ward[b] and P.A.J. de Groot[a]

[a]*School of Physics and Astronomy, University of Southampton, SO17 1BJ, United Kingdom*
[b]*Clarendon Laboratory, Oxford University, OX1 3PU, United Kingdom*

The properties of magnetic exchange springs states in epitaxial-grown (110)-$DyFe_2/YFe_2$ multilayers, with a1/4 ratio, for fields directed along a hard $[\bar{1}10]$ magnetic axis, are presented and discussed.

## 1. Introduction

It is known that $YFe_2$ dominated exchange spring $DyFe_2/YFe_2$ multilayers exhibit negative coercivity. In the presence of a high magnetic field, directed along an easy in-plane Dy [001]-axis, magnetic exchange springs form in the soft $YFe_2$ layers. Here the net magnetic moment is maximized because the Dy magnetic moments and those of the Fe atoms in the $YFe_2$ springs act in unison. However as the field is reduced, the $YFe_2$ springs unwind leading to a man-made net AF state in zero-field, with a negative magnetic moment [1].

Recent measurements on a [$DyFe_2$ (40Å) / $YFe_2$ (160 Å)] x 40 multilayer with a one-to-four ratio, at 50-100 K, with the field applied along a magnetically hard $[\bar{1}10]$ in-plane axis, show remarkably similar magnetization curves to those obtained along the easy [001] in-plane axis, despite out-of-plane behaviour [2]. This can be understood in terms of a strong local minimum in the anisotropy surface of the $Dy^{3+}$ atom lying near an out-plane [010]-axis ($\theta \approx$ 45°). Such an interpretation is supported by (i) neutron studies [2] and (ii) micro-magnetic simulations of the exchange spring system, given below. But, although the magnetization curves are almost identical, the two spin-configurations are very different.

## 2. Sample preparation

Details of the MBE crystal growth of the $REFe_2$ films have been given by [3,4]. The films are grown epitaxially on polished sapphire $(11\bar{2}0)$ substrates, coated initially with Nb and Fe seed layers. At 900 °C the Fe alloys with the Nb to form a Nb/Fe alloy which acts as a template for the $REFe_2$ layers. The $DyFe_2$ and $YFe_2$ layers are subsequently grown a-top the Nb/Fe layer at a temperature of 600 °C. Finally, on cooling down to room temperature, the films become uniformly strained due to substrate clamping. This occurs because the sapphire has a lower thermal expansion coefficient than that of the $REFe_2$ film. The contraction is along the (110) film growth-axis, giving rise to a shear strain $\varepsilon_{xy}$ = -0.55 % [5].

## 3. Results

The magnetization loop for a [$DyFe_2$ (40Å) / $YFe_2$ (160 Å)] x 40 multilayer can be seen in Fig.1. This was obtained at a temperature of 50 K with the field applied along the hard in-plane $[\bar{1}10]$-axis. A similar result is obtained at 100 K, but with a reduced switching field. Rather surprisingly, the magnetic loop is almost identical to that obtained for fields applied along an easy in-plane [001] axis [1]. Nevertheless, as we shall demonstrate, the spin-configurations in the two cases are very different.

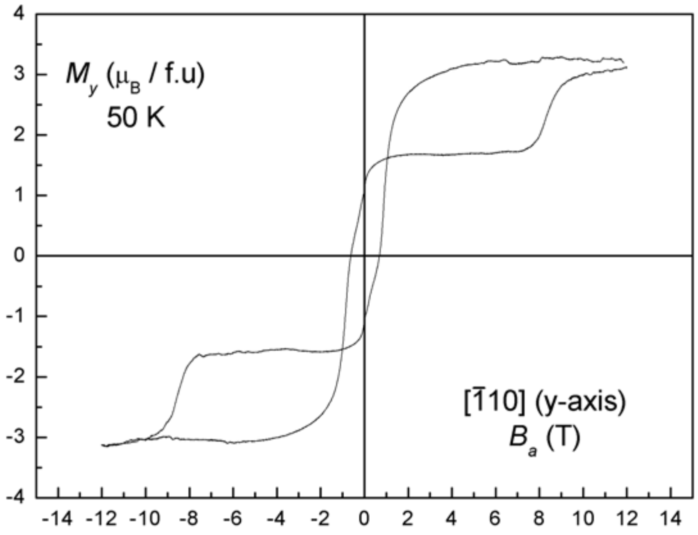


Fig. 1 Magnetization curve for $[DyFe_2\ (40Å)\ /\ YFe_2\ (160\ Å)] \times 40$ multilayer at 50 K for a field applied along a hard in-plane $[\bar{1}10]$ axis.

## 4. Micro-magnetic simulations

Details of the micro-magnetic program used to compute the magnetization curves shown below can be found elsewhere [6]. The I/P parameters such as Fe and Dy magnetic moments, anisotropy parameters and magnetic exchange fields, all as a function of temperature, can also be found elsewhere [7-9]. It should be noted that all the parameters used have been obtained from other experiments. They have not been manipulated to fit the magnetization data shown above.

The computed magnetization curves for the situation depicted in Fig. 1 can be seen in Fig. 2. From a comparison between Fig. 1 and Fig. 2, it will be seen that the agreement is very reasonable.

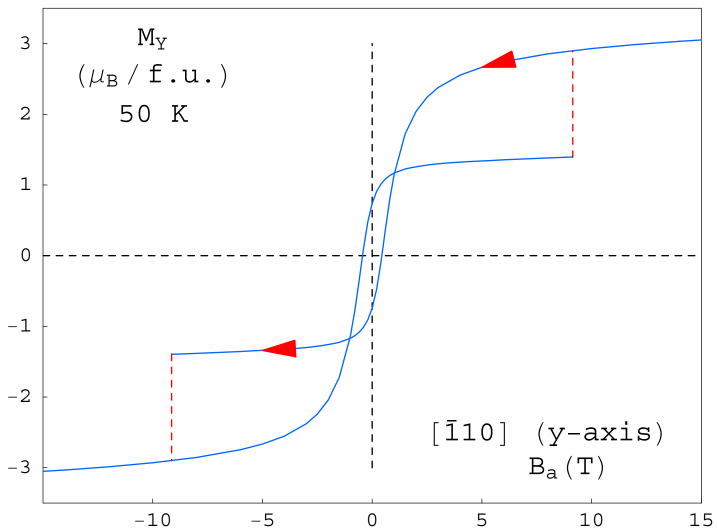


Fig. 2 Computed magnetization curve at 50 K

Nonetheless, as stated earlier, the two spin-configurations are very different. Examples can be seen in Fig. 3(a,b), in an applied field of 8 T. For the $[\bar{1}00]$-field results, the spins form a simple AF state where the spins are all confined to the plane of the film. However for the $[\bar{1}10]$ results, the Dy spins point out of plane, taking advantage of an out-of-plane [010] axis. Note the ‘spring’ in the $YFe_2$ layer, as the Fe spins strive to align themselves with the magnetic field.

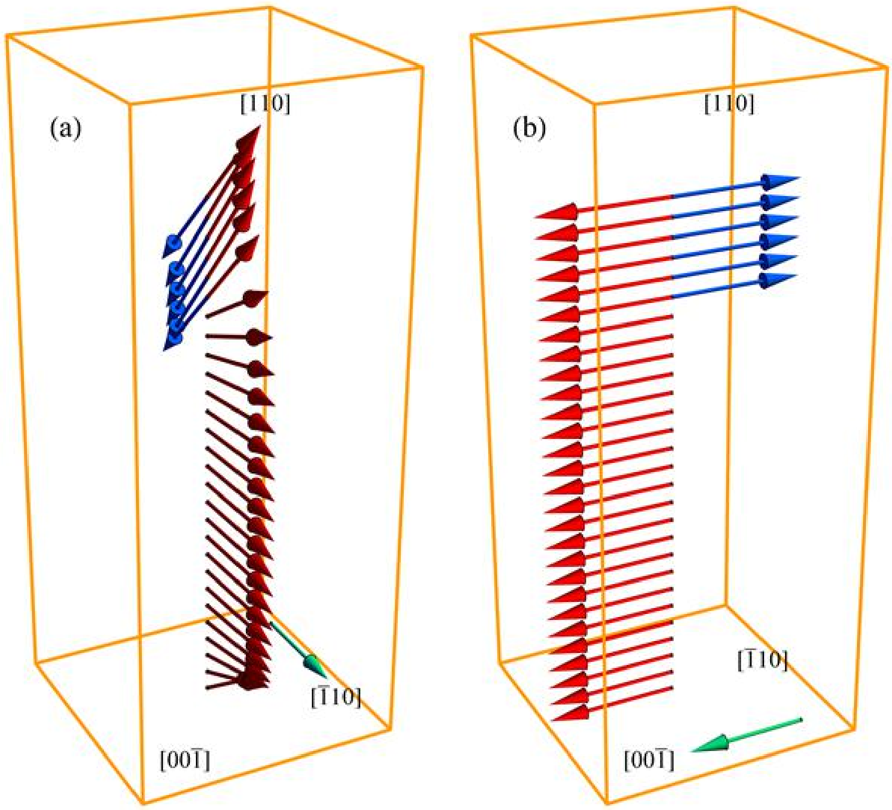


Fig. 3 Schematic representations of the spin-configurations for fields applied along the (a) $[\bar{1}10]$ and (b) $[00\bar{1}]$ axes, respectively, in a field of -8 T. The blue (red) arrows represent Dy (Fe) atoms, respectively. The green arrows indicate the direction of the magnetic field.

To understand why the spin–configuration for fields applied along the $[\bar{1}10]$-axis are stable, it is instructive to examine the anisotropy surface of the $Dy^{3+}$ ion at 50 K, shown in Fig. (4). It is immediately apparent from an examination of Fig. 4 that the $[\bar{1}10]$-axis represents a hard magnetic axis at 50 K, even though there is a slight indention in the surface. However, it is also obvious that the Dy spins can take advantage of an easy out-of-plane [010] cubic axis. In practice, therefore the Dy spins become trapped in the [010] local minimum. Out-of-plane behaviour is therefore inevitable. This is borne out by both neutron experiments [2], and the micro-magnetic simulations of the magnetization loops, detailed above.

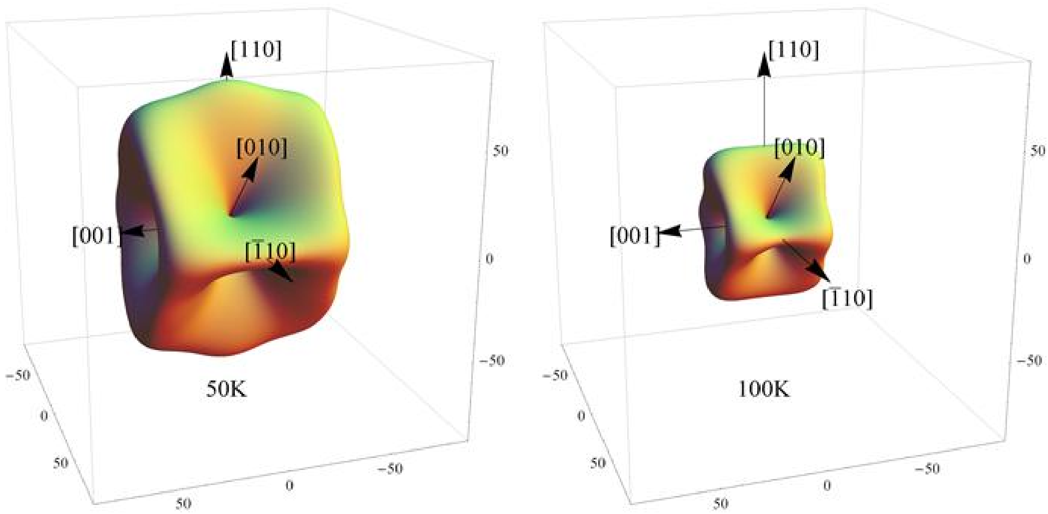


Fig. 4 Crystal field anisotropy surface for the $Dy^{3+}$ ion at 50 K and 100 K.

**Acknowledgments**

The support of the Engineering and Physical Sciences Research Council (EPSRC) is acknowledged.

**References**

[1] Bowden G J, Beaujour J-M L, Zhukov A A, Rainford B D, de Groot P A J, Ward R C C and Wells M R 2003 *J. App. Phys.* **93** 6480-2
[2] Bentall M J, Cowley R A, Buyers W J L, Tun Z, Lohstroh W, Ward R C C and Wells M R 2003 *J. Phys.: Condens. Matt. Phys.* **15** 4301-4330
[3] Bentall M J, Ward R C C, Grier E J and Wells M R 2003 *J. Phys.: Condens. Matt. Phys.* **15**, 6493
[4] Wang C, Kohn A, Wang S G and Ward R C C 2011 *J. Phys.: Condens. Matter* **23** 116001
[5] Mougin A, Dufour C, Dumesnil K and Mangin Ph 2000 *Phys. Rev. B* **62** 9517-9531
[6] Bowden G J, Martin K N, Rainford B D and de Groot P A J 2008 *J. Phys.: Condens. Matter* **20** 015209
[7] Bowden G J, Buckingham A R, Stenning G B G and de Groot P A J 2010 *Condens. Matt. Phys.* **22** 291001
[8] Bowden G J, Martin K N, Rainford B D and de Groot P A J 2008 J. *Phys: Condens. Matter* **20** 015209
[9] Stenning G B G, Buckingham A R, Bowden G J, Ward R C C, van der Laan G, Shelford L R, Maccherozzi F, Dhesi S S and de Groot P A J 2011 *Phys. Rev. B* **84** 104428